AGU PUBLICATIONS

Geophysical Research Letters

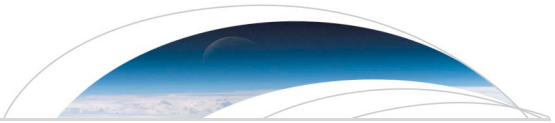

RESEARCH LETTER
10.1002/2015GL066515

Key Points:
- CryoSat-2 provides 92.3% ice shelf coverage, greater than any previous data set
- Mean elevation bias reduced from previous product, particularly in the key grounding zone
- Amery shelf grounding zone mean difference of 3.3% when compared to radio echo sounding data

Supporting Information:
- Figures S1–S4 and Captions for Tables S1–S3
- Table S1
- Table S2
- Table S3

Correspondence to:
S. J. Chuter,
s.chuter@bristol.ac.uk

Citation:
Chuter, S. J., and J. L. Bamber (2015), Antarctic ice shelf thickness from CryoSat-2 radar altimetry, *Geophys. Res. Lett.*, *42*, 10,721–10,729, doi:10.1002/2015GL066515.

Received 8 OCT 2015
Accepted 1 DEC 2015
Accepted article online 10 DEC 2015
Published online 23 DEC 2015

Antarctic ice shelf thickness from CryoSat-2 radar altimetry

S. J. Chuter[1] **and J. L. Bamber**[1]

[1]Bristol Glaciology Centre, School of Geographical Sciences, University of Bristol, Bristol, UK

Abstract Ice shelf thickness for the whole of Antarctica is derived from 4 years (2011–2014) of CryoSat-2 (CS2) radar altimetry measurements using the assumption that the shelves are in hydrostatic equilibrium. The satellite orbit and novel synthetic aperture radar interferometric mode of CS2 results in 92.3% data coverage over the ice shelves, with particular improvements around the grounding zone. When compared to ICESat data, surface elevations have a mean bias of less than 1 m and a fourfold reduction in standard deviation compared with the previous data set. Over the Amery Ice Shelf there is a mean thickness difference of 3.3% between radio echo sounding measurements and the CS2-derived thicknesses, rising to 4.7% within 10 km of the grounding line. Our new data set provides key improvements in accuracy and coverage, especially in the grounding zone, allowing for reduced uncertainties in mass budget calculations, subshelf ocean and ice sheet-shelf modeling.

1. Introduction

Ice shelves fringe a large proportion of the Antarctic continent, providing buttressing and stability to the interior grounded ice sheet [*Scambos et al.*, 2004; *Schoof*, 2007]. This is particularly pertinent to the West Antarctic Ice Sheet due to its potential instability. In the Amundsen Sea Embayment region, ice shelf thickness has reduced by 18% since 1994 [*Paolo et al.*, 2015], resulting in inland thinning [*Shepherd et al.*, 2002; *Pritchard et al.*, 2009; *McMillan et al.*, 2014] and accelerated mass loss of the grounded ice sheet. Similarly, increases in velocity and thinning occurred post-collapse of the Larsen B Ice Shelf in 2002 [*Scambos et al.*, 2004; *Rott et al.*, 2011].

Accurate quantification of ice shelf thickness close to the grounding line is required for ice sheet mass balance calculations using the mass budget method where direct measurements do not exist [*Rignot et al.*, 2008], which encompasses about 30% of the total grounding zone of outlet glaciers and ice streams [*Depoorter et al.*, 2013a]. Errors in ice thickness and surface mass balance currently constitute the largest uncertainty in mass budget calculations [*Shepherd et al.*, 2012]. Ice shelf thickness is also used in combination with bathymetry as a key boundary condition in subshelf ocean models [*Padman et al.*, 2002; *Timmerman et al.*, 2010; *Schodlok et al.*, 2012]. Sub-ice shelf cavity geometries regulate the access of Circumpolar Deep Water to the grounding line [*Jenkins et al.*, 2010], and oceanic forcing is a major driver of ice shelf mass loss [*Depoorter et al.*, 2013a]. Additionally, knowledge of ice thickness is required for buttressing parameterizations in ice sheet models [*De Rydt et al.*, 2015]. For mass balance and modeling applications, radio echo sounding (RES) measurements of ice thickness do not provide spatial coverage at the continental scale. To overcome this issue, freeboard measurements from satellite radar altimetry have been used, based on the assumption that the shelf is in hydrostatic equilibrium (HE) with the ocean [*Bamber and Bentley*, 1994; *Griggs and Bamber*, 2009b, 2011].

Both the orbital characteristics (repeat period and inclination) and operating modes of CryoSat-2 (CS2) mean that coverage over the ice shelves and, in particular, the grounding zone is greatly enhanced compared with previous altimeter missions [*Wang et al.*, 2015]. As a result, it provides the capability to significantly improve the previous continental-scale data set [*Griggs and Bamber*, 2011], which constitutes the ice shelf component of the widely used Bedmap2 data set for Antarctica [*Fretwell et al.*, 2013].

2. Data

Four years of CS2 (January 2011 to December 2014) synthetic aperture radar interferometric (SARIn) L2i Baseline B mode surface elevation measurements are used to create an ice shelf digital elevation model (DEM), from which thickness is calculated. CS2 was specifically designed to monitor the Earth's polar regions, providing coverage up to 88° south in a 369 day repeat cycle [*Drinkwater et al.*, 2004; *Wingham et al.*, 2006]. This results in a high data density with across-track spacing of 2.5 km at 70°. The SARIn mode also overcomes

the "loss-of-lock" issue experienced by previous radar altimetry missions close to areas where there is a break in slope, typical of the grounding zone [*Bamber et al.*, 2009]. This is achieved through beam focusing using dual antennae operating in an interferometric mode. This also negates the need for a slope correction to be applied to the data during post-processing. To avoid introducing biases in elevations close to the grounding line, we masked out all data over grounded ice using a new, complete grounding line mask [*Depoorter et al.*, 2013b], which combines parts of several previous data sets [*Scambos et al.*, 2007; *Brunt et al.*, 2010; *Bindschadler et al.*, 2011; *Rignot et al.*, 2011].

Erroneous elevation measurements were removed in two main stages. First, measurements were compared to a previous Antarctic DEM [*Griggs and Bamber*, 2009a], with points falling outside a ±150 m threshold (3 times the maximum RMS of the DEM, with allowance for $\Delta h/\Delta t$ between data sets) removed. Second, an iterative 3σ filter was applied at a 5 km resolution to remove outliers. Points <5 m in elevation with respect to the EIGEN-6C4 Geoid [*Förste et al.*, 2014] were also removed to ensure that data that might be over sea ice were not included. After these procedures, 94% of the data were left for interpolation. Tidal corrections were applied using the CATS2008a model [*Padman et al.*, 2002, 2008].

3. Methods

CS2 elevation measurements were gridded onto a 1 km quasi-regular polar stereographic grid. A quasi-regular grid was used to account for nonuniform spatial distribution of elevation measurements within each grid cell. The orbital characteristics and SARIn mode of operation have resulted in high-density coverage, with only 7.3% of grid cells requiring interpolation (i.e., having no valid observations in them).

The inverse distance weight (IDW) method of interpolation was used with a 50 km search radius. Each ice shelf was interpolated separately to avoid interpolation artifacts across adjacent shelves. Due to the topographically homogeneous nature of the ice shelves, having slopes typically less than 0.2°, and the high spatial density of data, the IDW method is an effective interpolation approach.

The assumption of HE allows for the calculation of ice thickness from the freeboard determined from the surface DEM:

$$z = \frac{(e-\delta)\rho_w}{\rho_w - \rho_i} + \delta$$

where Z is the actual ice thickness, e is the freeboard of the ice shelf above mean sea level, δ is the air content of the firn layer expressed in meters of ice equivalent, ρ_w is the water density underneath the ice shelf, and ρ_i is the ice density. Densities of 917 kg m^3 and 1027 kg m^3 were used for ρ_i and ρ_w, respectively. The ice density used is the mean value observed across the Amery Ice Shelf [*Fricker et al.*, 2001].

Ellipsoidal surface elevations were converted to freeboard measurements using the EIGEN-6C4 Geoid [*Förste et al.*, 2014], resampled to a 1 km grid from its original resolution of 9 km. We correct for changes in ocean surface height from nontidal effects using the DTU12MDT mean dynamic topography (MDT) data set [*Knudsen and Andersen*, 2012]. As MDT is not directly measurable over the ice shelves, values at the ice shelf front were extrapolated across the whole ice shelf. Due to high spatial variability in MDT over short spatial scales in the Southern Ocean [*Griesel et al.*, 2012], no correction was applied over the Ross, Filchner-Ronne, and Amery Ice Shelves as their size means they have their own subshelf circulation regime. This lack of correction equates to an approximate maximum 18 m error in thickness measurement.

To account for the layer of variable density firn at the surface of the ice shelf, firn air depth content was estimated from a firn densification model [*Ligtenberg et al.*, 2011, 2014], forced by the RACMO2.3 regional climate model. The firn model is time dependent and includes surface melt processes, from which we used the 2011–2013 mean model values. The native 27 km resolution of the model was resampled to a 1 km grid spacing. High-resolution (3 km spacing) airborne RES observations of firn air content were available for the Larsen C Ice Shelf [*Holland et al.*, 2011] and were used in this region instead of modeled values.

4. Results

The orbital and instrument properties of CS2 have resulted in major improvements in data coverage in comparison to the previous data set with increases of over 50% for several of the smaller ice shelves such

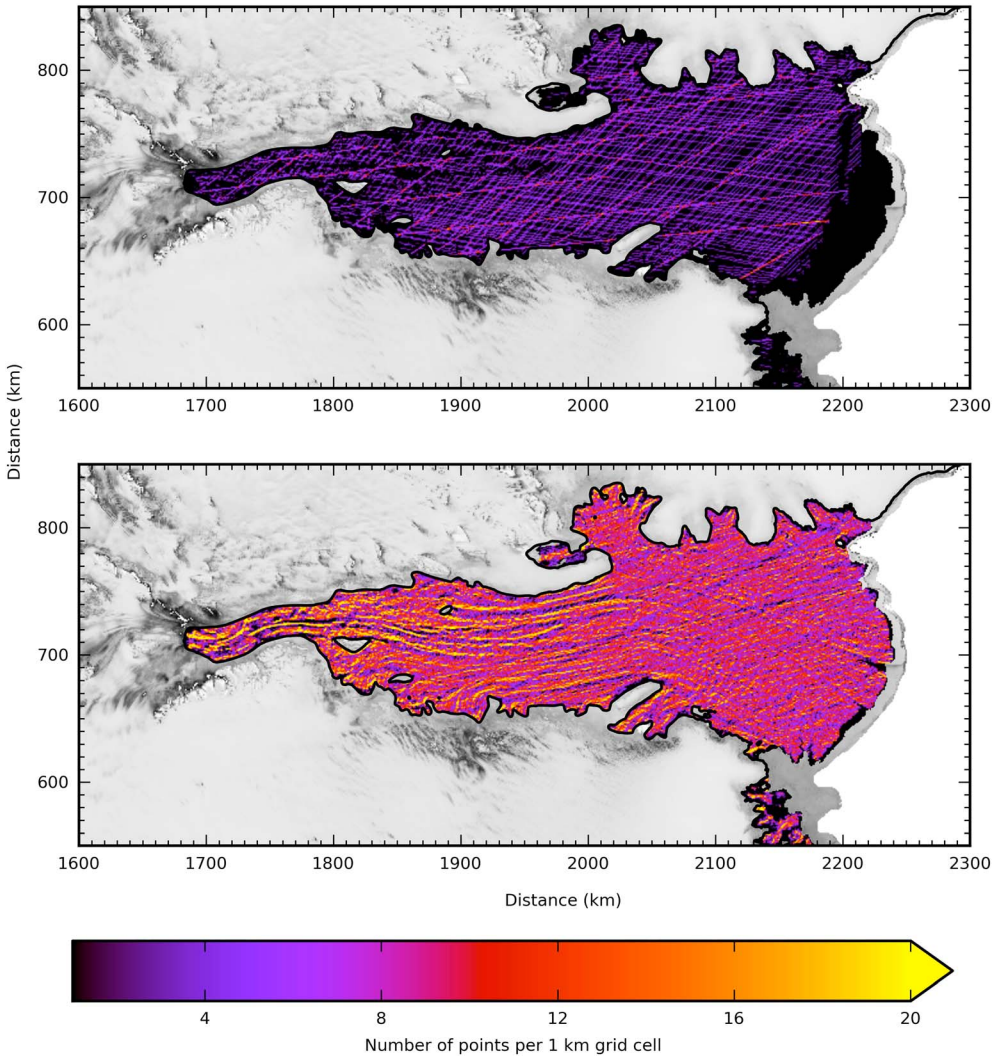

Figure 1. Number of surface elevation measurements per 1 km grid cell across the Amery Ice Shelf. (top) ERS-1 and ICESat coverage provided for the previous continental ice shelf thickness data set [*Griggs and Bamber*, 2011]. (bottom) CryoSat-2 coverage used in the new data product. The grounding line is shown in black [*Depoorter et al.*, 2013b], and data are overlain on the 2009 Mosaic of Antarctica (MOA) [*Haran et al.*, 2014].

as Venable and Totten (Table S1 in the supporting information), but also south of 81.5° for the two largest shelves: the Ross and Filchner-Ronne. This improved data coverage is illustrated for the Amery Ice Shelf (Figure 1), where coverage has increased by 44% from the previous Antarctic-wide data set [*Griggs and Bamber*, 2011]. Improved coverage is particularly evident close to the grounding line: a boundary that is important for ice sheet-shelf modeling and for mass budget calculations.

Accuracy assessment of the DEM was undertaken by calculating differences from the Geoscience Laser Altimeter System aboard the NASA ICESat satellite. These data have a small spatial footprint (70 m) and minimal firn penetration of the laser. Release 34 GLA12 data from all campaigns (2003–2009) were used in the comparison in order to ensure maximum data availability. The same quality control procedures used for the CS2 data were applied to the ICESat data, with a tidal correction applied from the CATS2008a tide model [*Padman et al.*, 2002, 2008]. To account for temporal changes in surface elevation between the data sets, a $\Delta h/\Delta t$ correction was applied to the ICESat measurements [*Paolo et al.*, 2015]. These corrections are of a relatively high temporal resolution (3-monthly) over an 18 year period (1994–2012).

Mean differences (ICESat-CS2) across the largest ice shelves (Table S2) indicate a general positive bias between ICESat measurements and the CS2 DEM. The mean difference across the whole continent is less than 1 m, meaning that the bias in the CS2 elevations contributes on average <9 m to the thickness error.

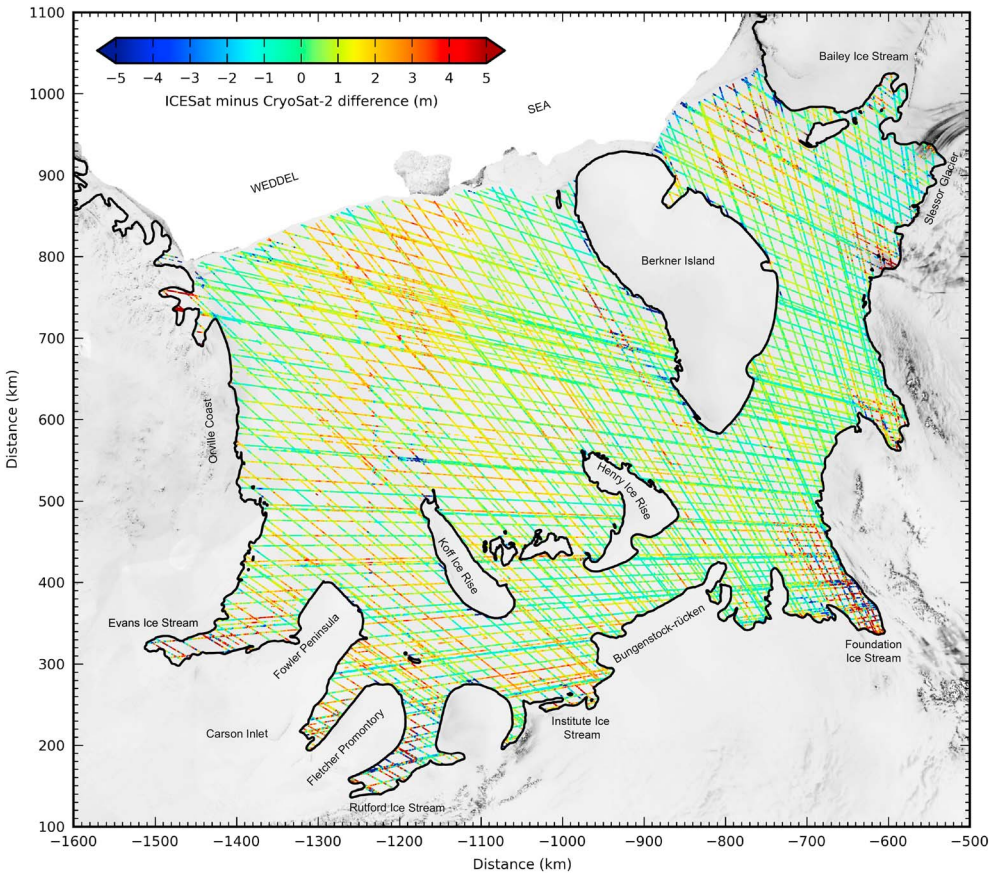

Figure 2. Comparison of ICESat elevation measurements with the CryoSat-2 ice shelf DEM (ICESat-CS2) over the Filchner-Ronne Ice Shelf. Differences are calculated through bilinear interpolation of the ICESat surface elevation measurement to the CS2 DEM. The grounding line is shown in black [*Depoorter et al.*, 2013b] and overlain on the 2009 MOA [*Haran et al.*, 2014].

One explanation for the bias is that it is due to the propagation of the CS2 microwave signal into the firn layer, resulting in lower surface elevation measurements. The effect of firn penetration varies spatially, with penetration depth likely being a function of firn density [*Wang et al.*, 2015].

There are substantial improvements over the previous Antarctic-wide data set, with a reduction in both mean bias and a fourfold reduction in standard deviation on average across the continent. The greatest reductions are shown within 10 km of the grounding line, with an absolute reduction of 22 m in standard deviation compared to the previous data set. These improvements can be attributed to an increase in data coverage and density, in particular over the grounding zone where the SARIn mode alleviates the off-ranging and loss-of-lock problems associated with conventional radar altimetry.

The Filchner-Ronne Ice Shelf (Figure 2) illustrates these results, with differences generally below 1 m across the whole ice shelf. Differences around the grounding line are also generally within 1 m, highlighting the performance capabilities of the SARIn mode. Differences are larger in the vicinity of Foundation Ice Stream, which was not covered by the SARIn mode mask until 2013. As a result, this section of the ice shelf only has coverage from one pass, leading to reductions in data density in this locality.

Validation of the CS2-derived ice shelf thickness data has been undertaken through comparison with airborne RES measurements, with differences calculated via bilinear interpolation of RES measurements to the ice thickness grid (RES-CS2). Validation was undertaken using RES data from multiple campaigns (Table S3). The SOAR/CASSERTZ (US Support Office for Aerogeophysical Research–Corridor Aerogeophysics of the South East Ross Transect Zone) [*Blankenship et al.*, 2001] and West Marie Byrd (WMB) [*Luyendyk and Wilson*, 2003] Land surveys were both also used as validation data sets for the previous continental data set [*Griggs and Bamber*, 2011], allowing for a direct comparison between the two thickness data sets. For the

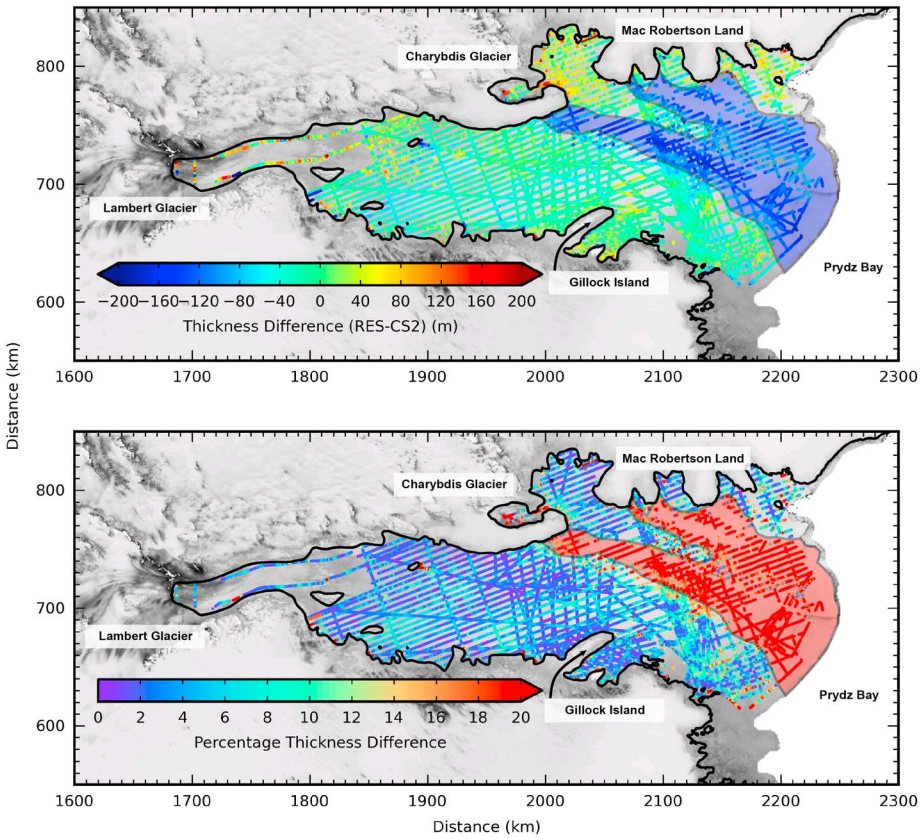

Figure 3. Thickness validation over the Amery Ice Shelf using ANARE RES data. (top) Absolute differences between the data sets. (bottom) Absolute percentage differences between the two data sets. The blue and red overlay regions define the extent of the marine ice, with all points in this region being excluded from the validation. These regions of marine ice are in agreement with previous marine ice mapping over the Amery Ice Shelf [*Fricker et al*., 2001; *Craven et al*., 2009]. Data are overlain on the 2009 MOA [*Haran et al*., 2014], and the grounding line is shown in black [*Depoorter et al*., 2013b].

SOAR/CASSERTZ data set (Figure S2) over the Ross Ice Shelf, the mean bias and standard deviation have reduced by 5.05 m and 19.11 m respectively. Over the WMB region, large improvements in performance can be seen with a tenfold decrease in the mean bias and an approximate threefold decrease in standard deviation.

5. Discussion

Extensive high spatial density RES measurements exist across the Amery Ice Shelf, provided by the Australian National Antarctic Research Expedition (ANARE). As a result, it allows for a more complete validation to be undertaken for this shelf. The data have a thickness accuracy range of 75 to 30 m and a positional accuracy range of 100 to 20 m. Only data from acquisition campaigns carried out between 1990 and 2004 were used, as data from earlier campaigns have larger uncertainties in both thickness and location. Temporal changes in thickness are small on this ice shelf with a 1.6 ± 1.1 m increase in thickness per decade [*Paolo et al*., 2015]. Therefore, no $\Delta T/\Delta t$ correction was applied as this rate of change is smaller than other known errors in thickness.

There is a mean bias and standard deviation between the data sets of -0.58 m and 33.4 m, respectively (excluding measurements from regions of marine ice), implying that the CS2 thickness product is on average thicker than the RES measurements for the Amery Ice Shelf. Over the whole of the ice shelf, these differences equate to a mean absolute 3.3% error across the ice shelf (Figure 3). Examining differences within 10 km of the grounding line, the mean bias becomes 5.79 m and standard deviation 56.4 m, equating to a 4.7% error in ice thickness. Errors in previous HE-derived ice thickness at the grounding line range from about 10 to 15% [*Depoorter et al*., 2013a]. Based on this analysis, our new product is, therefore, between 2 and 3 times more accurate across the Amery Ice Shelf. The increase in standard deviation within the grounding

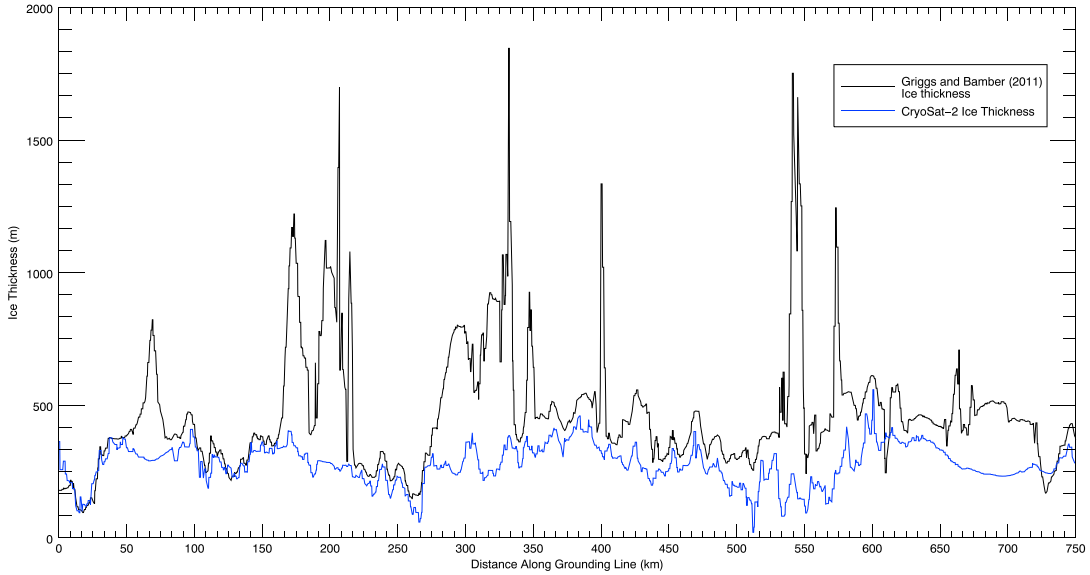

Figure 4. Ice thickness at the grounding line of the Abbot Ice Shelf (see Figure S1 for location) for both the CS2 ice thickness product (blue) and the previous continental ice shelf thickness data set (black) [*Griggs and Bamber*, 2011]. Our CS2 ice thickness product has a mean 29% reduction in thickness compared to the previous data set. Additionally, the CS2 product does not suffer from the data spikes of the previous product, due to the improved performance of CS2 within the grounding zone.

zone is very likely due to the breakdown of the HE assumption close to the grounding line. It may also be due to localized differences in firn air content due to ice dynamics [*Bamber and Bentley*, 1994].

The spatial clustering of large negative differences (>20% thickness error) extending from the grounding line of the Charybdis Glacier to the calving front is likely due to the presence of marine ice accreting to the base of the ice shelf, collocating with previous estimated locations [*Fricker et al*., 2001]. These large differences are caused by RES echoes reflecting off the marine/meteoric ice interface as opposed to the ice/ocean interface, a result of the increase in salinity [*Oerter et al*., 1992] and density of the marine ice [*Craven et al*., 2009]. Marine ice in this area can be over 200 m thick and form approximately 40% of the total ice thickness near the calving front [*Craven et al*., 2009]. The differing densities of the meteoric and marine ice introduce errors into the CS2-derived thicknesses, due to the use of a single ice density value in the calculation. Marine ice has been observed to have a maximum density of 938 kg m^{-3}, causing a 5% thickness error when occupying half the ice column [*Griggs and Bamber*, 2011]. Similar spatial clustering of large negative differences has been found over the Filchner-Ronne Ice Shelf (Figure S4), also linked to where previous studies have proposed the existence of marine ice [*Joughin and Vaughan*, 2004; *Lambrecht et al*., 2007].

There is a large spatial variability in the air content of the firn layer over the Amery Ice Shelf, from 0 m toward the southernmost region of the grounding line (Lambert Glacier grounding line) to a maximum of 19.7 m. Areas where no firn layer is present are due to katabatic wind sublimation processes and seasonal melt [*Parish and Bromwich*, 1987; *Scambos et al*., 2012], which exceeds the accumulation rate at a given location. Wind- and melt-driven "blue ice" areas have been observed over the Amery Ice Shelf with satellite imagery [*Winther et al*., 2001], potentially extending as far north to Gillock Island from the Lambert Glacier grounding line. The inclusion of melt processes in the time-dependent firn model [*Ligtenberg et al*., 2014] is valuable in accurately representing these processes.

When we use a steady state firn densification model without melt processes [*van den Broeke*, 2008] in our calculations (the same model used in the previous data set), the mean percentage error in thickness increases to 10.3% across the whole shelf and 23.5% within 10 km of the grounding line. The use of the new firn densification model leads, therefore, to a fourfold reduction in absolute percentage ice thickness error in the grounding zone, subsequently allowing for greater constraint of errors in ice discharge calculations. Previous steady state models have overestimated firn air content at the grounding line by 2.7 m compared to the model used in our calculations [*Ligtenberg et al*., 2014], equating to a 28 m error in derived thickness at the grounding line.

Sub-ice shelf channels exist close to the Lambert Glacier grounding line, caused by the suture of ice streams [*Le Brocq et al*., 2013]. These channels across the ice shelf can be up to 500 m deep and 1.5 km in width [*Fricker et al*., 2009]. The width of these channels means that they are, at least in part, captured by the 1 km resolution of the product and are expressed by localized depressions in surface elevation. However, narrow channels can experience bridging stresses, which act to prevent the ice from fully hydrostatically adjusting in accordance with the change in thickness caused by the channel [*Drews*, 2015]. As a result, these channels cannot be captured using the HE assumption, causing errors at the localized (subkilometer) scale.

The improvement in accuracy at the GL provided by the CS2 data set is illustrated for the Abbot Ice Shelf (Figure S1). This is a sector where HE-derived ice thickness has been used in input-output mass balance estimates due to the absence of measured thickness data. Over this ice shelf, our new data have a mean reduction in ice thickness at the grounding line of 29% compared to the previous data set (Figure 4). This reduction in thickness results in a change in mass balance from $-14 \pm 9\,\mathrm{Gt\,yr^{-1}}$ [*Rignot et al*., 2008] to approximately $-4 \pm 9\,\mathrm{Gt\,yr^{-1}}$, for the same epoch. This near-zero mass balance is more consistent with satellite altimetry measurements that has a slightly positive elevation rate over the period 1995–2005 [*Rignot et al*., 2008]. In addition, the new data set shows reductions in both noise and "data spikes" close to the grounding line (Figure 4). This is a result of the increased data density and improved performance provided by the SARIn mode of CS2. The use of the new ice thickness data will result in greatly improved input-output method mass balance estimates for approximately one third of the grounding line where direct measurements of ice thickness do not exist.

5. Conclusions

A new 1 km ice shelf DEM and thickness data set has been calculated using 4 years of CS2 surface elevation measurements. Data coverage has improved by over 50% over several ice shelves, due to the dense across-track spacing and the alleviation of the loss-of-lock issues which have hampered previous satellite radar altimeter missions. Validation of the DEM with ICESat laser altimetry elevation measurements a mean bias of 0.56 m over all shelves, with fourfold reductions in standard deviation compared to the previous continental data set. The greatest absolute reductions are generally found within 10 km of the grounding zone.

Thickness measurements were validated against several RES campaign data sets, with improvements in both mean bias and standard deviation where the same data set was also used in the validation of the previous data product. Analysis over the Amery Ice Shelf shows a mean thickness difference of 3.3%, increasing to 4.7% in the grounding zone. Large negative absolute differences highlight areas of marine ice accretion at the base of the ice shelf, offering the potential for future marine ice mapping applications. The use of a firn densification model that incorporates surface melt processes more accurately captures the complex firn processes in this region compared to the steady state model used in the previous data set, leading to significant improvements in accuracy.

Our results will allow for improved errors in mass balance calculations using the mass budget or input-output method, as demonstrated over the Abott Ice Shelf. Additionally, it allows for more accurate parameterizations of sub-ice shelf ocean and ice sheet models. This data set provides an important advance to the data used in the Bedmap2 product. The previous ice shelf thickness data set was adjusted to match grounded ice thickness observations in Bedmap2 [*Fretwell et al*., 2013]. We expect considerably improved consistency between our new product and grounded ice thickness observations, reducing the need for ad hoc, manual adjustment. There may, however, be biases for some sectors due to the breakdown in the HE assumption close to the grounding line. The RES validation data used here did not suggest the presence of such biases, but their coverage is insufficient to fully investigate this issue. This is the subject of further work. The product will be made publically available to the community.

Acknowledgments
This work was supported by the UK Natural Environment Research Council (NERC) grant NE/I027401/1. The European Space Agency (ESA) provided the CryoSat-2 data used for this research. ICESat data used were provided by NASA and are available from the National Snow and Ice Data Center. We thank M.A. Depoorter for the grounding line and ice shelf mask and F. Paolo for providing the $\Delta h/\Delta t$ correction used in the elevation validation. We also thank S. Ligtenberg and P. Holland for providing the firn density correction. We also thank all of the RES data providers: NASA's Operation Ice Bridge, British Antarctic Survey, University of Texas Institute of Geophysics, and the Australian National Antarctic Research Expedition. We would like to thank the two anonymous reviewers for their comments when evaluating this paper.

References

Bamber, J., and C. R. Bentley (1994), A comparison of satellite-altimetry and ice-thickness measurements of the Ross Ice Shelf, Antarctica, *Ann. Glaciol.*, *20*, 357–364, doi:10.3189/172756494794587582.

Bamber, J. L., J. L. Gomez-Dans, and J. A. Griggs (2009), A new 1 km digital elevation model of the Antarctic derived from combined satellite radar and laser data—Part 1: Data and methods, *Cryosphere*, *3*(1), 101–111, doi:10.5194/tc-3-101-2009.

Bindschadler, R., H. Choi, and A. Collaborators (2011), High-resolution image-derived grounding and hydrostatic lines for the Antarctic ice sheet, doi:10.7265/N56T0JK2.

Blankenship, D. D., D. L. Morse, C. A. Finn, R. E. Bell, M. E. Peters, S. D. Kempf, S. M. Hodge, M. Studinger, J. C. Behrendt, and J. M. Brozena (2001), Geologic controls on the initiation of rapid basal motion for West Antarctic ice streams: A geophysical perspective including new airborne radar sounding and laser altimetry results, in *The West Antarctic Ice Sheet: Behavior and Environment*, pp. 105–121, AGU, Washington, D. C.

Brunt, K. M., H. A. Fricker, L. Padman, T. A. Scambos, and S. O'Neel (2010), Mapping the grounding zone of the Ross Ice Shelf, Antarctica, using ICESat laser altimetry, *Ann. Glaciol.*, *51*(55), 71–79.

Craven, M., I. Allison, H. A. Fricker, and A. R. Warner (2009), Properties of a marine ice layer under the Amery Ice Shelf, East Antarctica, *J. Glaciol.*, *55*(192), 717–728, doi:10.3189/002214309789470941.

Depoorter, M. A., J. L. Bamber, J. A. Griggs, J. T. M. Lenaerts, S. R. M. Ligtenberg, M. R. van den Broeke, and G. Moholdt (2013a), Calving fluxes and basal melt rates of Antarctic ice shelves, *Nature*, *502*(7472), 580, doi:10.1038/nature12737.

Depoorter, M. A., J. L. Bamber, J. Griggs, J. T. M. Lenaerts, S. R. M. Ligtenberg, M. R. van den Broeke, and G. Moholdt (2013b), Synthesized grounding line and ice shelf mask for Antarctica, Supplement to Depoorter, M. A., J. L. Bamber, J. Griggs, J. T. M Lenaerts, S. R. M. Ligtenberg, M. R. van den Broeke, and G. Moholdt, Calving fluxes basal melt rates Antarctic ice shelves, *Nature*, *502*, 89–92, doi:10.1594/PANGAEA.819151.

De Rydt, J., G. H. Gudmundsson, H. Rott, and J. L. Bamber (2015), Modeling the instantaneous response of glaciers after the collapse of the Larsen B Ice Shelf, *Geophys. Res. Lett.*, *42*, 5355–5363, doi:10.1002/2015GL064355.1.

Drews, R. (2015), Evolution of ice-shelf channels in Antarctic ice shelves, *Cryosphere*, *9*(3), 1169–1181, doi:10.5194/tc-9-1169-2015.

Drinkwater, M. R., R. Francis, G. Ratier, and D. J. Wingham (2004), The European Space Agency's Earth Explorer Mission CryoSat: Measuring variability in the cryosphere, *Ann. Glaciol.*, *39*(1), 313–320.

Förste, C., et al. (2014), EIGEN-6C4—The latest combined global gravity field model including GOCE data up to degree and order 1949 of GFZ Potsdam and GRGS Toulouse, Geophysical Research Abstracts, vol. 16, EGU2014-3707, EGU General Assembly, Vienna.

Fretwell, P., et al. (2013), Bedmap2: Improved ice bed, surface and thickness datasets for Antarctica, *Cryosphere*, *7*(1), 375–393, doi:10.5194/tc-7-375-2013.

Fricker, H. A., S. Popov, I. Allison, and N. Young (2001), Distribution of marine ice beneath the Amery Ice Shelf, *Geophys. Res. Lett.*, *28*, 2241–2244, doi:10.1029/2000GL012461.

Fricker, H. A., R. Coleman, L. Padman, T. A. Scambos, J. Bohlander, and K. M. Brunt (2009), Mapping the grounding zone of the Amery Ice Shelf, East Antarctica using InSAR, MODIS and ICESat, *Antarct. Sci.*, *21*(5), 515–532, doi:10.1017/S095410200999023x.

Griesel, A., M. R. Mazloff, and S. T. Gille (2012), Mean dynamic topography in the Southern Ocean: Evaluating Antarctic Circumpolar Current transport, *J. Geophys. Res.*, *117*, C01020, doi:10.1029/2011JC007573.

Griggs, J. A., and J. L. Bamber (2009a), A new 1 km digital elevation model of Antarctica derived from combined radar and laser data—Part 2: Validation and error estimates, *Cryosphere*, *3*(1), 113–123.

Griggs, J. A., and J. L. Bamber (2009b), Ice shelf thickness over Larsen C, Antarctica, derived from satellite altimetry, *Geophys. Res. Lett.*, *36*, L19501, doi:10.1029/2009GL039527.

Griggs, J. A., and J. L. Bamber (2011), Antarctic ice-shelf thickness from satellite radar altimetry, *J. Glaciol.*, *57*(203), 485–498, doi:10.3189/002214311796905659.

Haran, T. M., J. A. Bohlander, T. A. Scambos, T. H. Painter, and M. A. Fahnestock (2014), MODIS Mosaic of Antarctica 2008–2009 (MOA2009) image map, doi:10.7265/N5KP8037.

Holland, P. R., H. F. J. Corr, H. D. Pritchard, D. G. Vaughan, R. J. Arthern, A. Jenkins, and M. Tedesco (2011), The air content of Larsen Ice Shelf, *Geophys. Res. Lett.*, *38*, L10503, doi:10.1029/2011GL047245.

Jenkins, A., P. Dutrieux, S. S. Jacobs, S. D. McPhail, J. R. Perrett, A. T. Webb, and D. White (2010), Observations beneath Pine Island Glacier in West Antarctica and implications for its retreat, *Nat. Geosci.*, *3*(7), 468–472.

Joughin, I., and D. G. Vaughan (2004), Marine ice beneath the Filchner-Ronne Ice Shelf, Antarctica: A comparison of estimated thickness distributions, *Ann. Glaciol.*, *39*, 511–517, doi:10.3189/172756404781814717.

Knudsen, P., and O. B. Andersen (2012), A global mean ocean circulation estimation using GOCE gravity models—The DTU12MDT mean dynamic topography model, in *20 Years of Progress in Radar Altimetry*, SP-710, 123 pp., European Space Agency ESA, Venice.

Lambrecht, A., H. Sandhäger, D. G. Vaughan, and C. Mayer (2007), New ice thickness maps of Filchner-Ronne Ice Shelf, Antarctica, with specific focus on grounding lines and marine ice, *Antarct. Sci.*, *19*(4), 521–532, doi:10.1017/S0954102007000661.

Le Brocq, A. M., et al. (2013), Evidence from ice shelves for channelized meltwater flow beneath the Antarctic Ice Sheet, *Nat. Geosci.*, *6*(11), 945–948, doi:10.1038/ngeo1977.

Ligtenberg, S. R. M., M. M. Helsen, and M. R. Van Den Broeke (2011), An improved semi-empirical model for the densification of Antarctic firn, *Cryosphere*, *5*(4), 809–819, doi:10.5194/tc-5-809-2011.

Ligtenberg, S. R. M., P. Kuipers Munneke, and M. R. van den Broeke (2014), Present and future variations in Antarctic firn air content, *Cryosphere*, *8*(1), 1711–1723, doi:10.5194/tcd-8-421-2014.

Luyendyk, B. P., and D. Wilson (2003), Surface elevation and ice thickness, Western Marie Byrd Land, Antarctica, doi:10.7265/N5BZ63ZH.

McMillan, M., A. Shepherd, A. Sundal, K. Briggs, A. Muir, A. Ridout, A. Hogg, and D. Wingham (2014), Increased ice losses from Antarctica detected by CryoSat-2, *Geophys. Res. Lett.*, *41*, 3899–3905, doi:10.1002/2014GL060111.

Oerter, H., J. Kipfstuhl, J. Determann, H. Miller, D. Wagenbach, A. Minikin, and W. Graf (1992), Evidence for basal marine ice in the Filchner-Ronne Ice Shelf, *Nature*, *358*, 399–401.

Padman, L., H. A. Fricker, R. Coleman, S. Howard, and L. Erofeeva (2002), A new tide model for the Antarctic ice shelves and seas, *Ann. Glaciol.*, *34*, 247–254, doi:10.3189/172756402781817752.

Padman, L., S. Y. Erofeeva, and H. A. Flicker (2008), Improving Antarctic tide models by assimilation of ICESat laser altimetry over ice shelves, *Geophys. Res. Lett.*, *35*, L22504, doi:10.1029/2008GL035592.

Paolo, F. S., H. A. Fricker, and L. Padman (2015), Volume loss from Antarctic ice shelves is accelerating, *Science*, *348*, 327–331, doi:10.1126/science.aaa0940.

Parish, T. R., and D. H. Bromwich (1987), The surface windfield over the Antarctic ice sheets, *Nature*, *328*(6125), 51–54.

Pritchard, H. D., R. J. Arthern, D. G. Vaughan, and L. A. Edwards (2009), Extensive dynamic thinning on the margins of the Greenland and Antarctic ice sheets, *Nature*, *461*(7266), 971–975, doi:10.1038/nature08471.

Rignot, E., J. L. Bamber, M. R. Van Den Broeke, C. Davis, Y. H. Li, W. J. Van De Berg, and E. Van Meijgaard (2008), Recent Antarctic ice mass loss from radar interferometry and regional climate modelling, *Nat. Geosci.*, *1*(2), 106–110, doi:10.1038/ngeo102.

Rignot, E., J. Mouginot, and B. Scheuchl (2011), Antarctic grounding line from differential satellite radar interferometry, *Geophys. Res. Lett.*, *38*, L10504, doi:10.1029/2011GL047109.

Rott, H., F. Muller, T. Nagler, and D. Floricioiu (2011), The imbalance of glaciers after disintegration of Larsen-B ice shelf, Antarctic Peninsula, *Cryosphere*, *5*(1), 125–134, doi:10.5194/tc-5-125-2011.

Scambos, T. A., J. A. Bohlander, C. A. Shuman, and P. Skvarca (2004), Glacier acceleration and thinning after ice shelf collapse in the Larsen B embayment, Antarctica, *Geophys. Res. Lett.*, *31*, L18402, doi:10.1029/2004GL020670.

Scambos, T. A., T. M. Haran, M. A. Fahnestock, T. H. Painter, and J. Bohlander (2007), MODIS-based Mosaic of Antarctica (MOA) data sets: Continent-wide surface morphology and snow grain size, *Remote Sens. Environ.*, *111*(2–3), 242–257, doi:10.1016/j.rse.2006.12.020.

Scambos, T. A., et al. (2012), Extent of low-accumulation "wind glaze" areas on the East Antarctic plateau: Implications for continental ice mass balance, *J. Glaciol.*, *58*(210), 633–647, doi:10.3189/2012JoG11J232.

Schodlok, M. P., D. Menemenlis, E. Rignot, and M. Studinger (2012), Sensitivity of the ice-shelf/ocean system to the sub-ice-shelf cavity shape measured by NASA Ice Bridge in Pine Island Glacier, West Antarctica, *Ann. Glaciol.*, *53*(60), 156–162, doi:10.3189/2012aog60a073.

Schoof, C. (2007), Ice sheet grounding line dynamics: Steady states, stability, and hysteresis, *J. Geophys. Res.*, *112*, F03S28, doi:10.1029/2006JF000664.

Shepherd, A., D. J. Wingham, and J. A. D. Mansley (2002), Inland thinning of the Amundsen Sea sector, West Antarctica, *Geophys. Res. Lett.*, *29*(10), 1364, doi:10.1029/2001GL014183.

Shepherd, A., et al. (2012), A reconciled estimate of ice-sheet mass balance, *Science*, *338*(6111), 1183–1189.

Timmerman, R., et al. (2010), A consistent dataset of Antarctic ice sheet topography, cavity geometry, and global bathymetry, *Earth Syst. Sci. Data*, *2*, 261–273, doi:10.5194/essd-2-261-2010.

Van den Broeke, M. R. (2008), Depth and density of the Antarctic firn layer, *Arct. Antarct. Alp. Res.*, *40*(2), 432–438, doi:10.1657/1523-0430(07-021)[BROEKE]2.0.CO;2.

Wang, F., J. L. Bamber, and X. Cheng (2015), Accuracy and performance of CryoSat-2 SARIn mode data over Antarctica, *IEEE Geosci. Remote Sens. Lett.*, *12*(7), 1516–1520, doi:10.1109/LGRS.2015.2411434.

Wingham, D. J., et al. (2006), CryoSat: A mission to determine the fluctuations in Earth's land and marine ice fields, *Adv. Space Res.*, *37*(4), 841–871.

Winther, J.-G., M. N. Jespersen, and G. E. Liston (2001), Blue-ice areas in Antarctica derived from NOAA AVHRR satellite data, *J. Glaciol.*, *47*(157), 325–334.